

Comparison of Current Optical Coherence Tomography Angiography Methods in Imaging Retinal Hemangioblastomas

Michael Reich¹, Andreas Glatz¹, Daniel Boehringer¹, Charlotte Evers¹, Moritz Daniel¹, Felicitas Bucher¹, Franziska Ludwig¹, Simone Nuessle¹, Wolf A. Lagrèze¹, Peter M. Maloca^{2,3}, Clemens Lange¹, Thomas Reinhard¹, Hansjuergen Agostini¹, and Stefan J. Lang¹

¹ Eye Center, Faculty of Medicine, University of Freiburg, Freiburg, Germany

² Institute of Molecular and Clinical Ophthalmology Basel (IOB), Basel, Switzerland

³ Moorfields Eye Hospital NHS Foundation Trust, London, UK

Correspondence: Stefan J. Lang, Killianstrasse 5, D-79106 Freiburg, Germany. e-mail: stefan.lang@uniklinik-freiburg.de

Received: April 9, 2020

Accepted: May 15, 2020

Published: July 8, 2020

Keywords: von Hippel-Lindau disease; retinal capillary hemangioblastoma; spectral domain optical coherence tomography angiography; swept-source optical coherence tomography angiography; OCT angiography

Citation: Reich M, Glatz A, Boehringer D, Evers C, Daniel M, Bucher F, Ludwig F, Nuessle S, Lagrèze WA, Maloca PM, Lange C, Reinhard T, Agostini H, Lang SJ. Comparison of current optical coherence tomography angiography methods in imaging retinal hemangioblastomas. *Trans Vis Sci Tech.* 2020;9(8):12. <https://doi.org/10.1167/tvst.9.8.12>

Purpose: To compare spectral-domain (SD) and swept-source (SS) optical coherence tomography angiography (OCTA) for imaging retinal capillary hemangioblastomas (RCHs) in von Hippel-Lindau disease (VHLD).

Methods: Prospective single-center cross-sectional study. Tumor size (TS) of perfused RCHs was assessed clinically in relation to the optic disc size. For both technologies, SD-OCTA and SS-OCTA, corresponding images with a scan size of $3 \times 3 \text{ mm}^2$ and $6 \times 6 \text{ mm}^2$, respectively, were overlaid according to the set of marker positions to determine the TS.

Results: From 200 patients with VHLD, 48 patients showed 84 RCHs. SD-OCTA images of 39 RCHs (46.4%) and SS-OCTA images of 48 RCHs (57.2%) were suitable for analysis. The average in OCTA-measured TS of $1.60 \pm 2.58 \text{ mm}^2$ (range, 0.01–10.43) was congruent to the clinically assessed TS in 81.3% of cases ($r = 0.86$, $P < 0.0001$). TS measured in SD-OCTA compared to SS-OCTA showed similar values and a high correlation (all $P < 0.0001$). Nevertheless, despite the similarities, a slight trend in SS-OCTA was observed whereby with increasing TS, an elevated TS was detected compared to SD-OCTA ($3 \times 3\text{-mm}^2$ scans: mean difference of $0.03 \pm 0.04 \text{ mm}^2$, $6 \times 6\text{-mm}^2$ scans: $0.08 \pm 0.19 \text{ mm}^2$). However, within the same imaging technology method, TS values almost did not differ (SD-OCTA: mean difference of $0.01 \pm 0.02 \text{ mm}^2$, SS-OCTA: $0.001 \pm 0.01 \text{ mm}^2$).

Conclusions: OCTA may serve as an additional tool for diagnosis and monitoring of RCHs. Nevertheless, due to the differences between the technologies, the values cannot be used interchangeably.

Translational Relevance: SD-OCTA and SS-OCTA are suitable to detect and monitor RCHs and provide a more detailed assessment about the TS than this is clinically possible.

Introduction

Optical coherence tomography angiography (OCTA) is a new noninvasive technique for imaging the microvasculature of the retina and choroid^{1,2} and has rapidly gained clinical acceptance.^{2,3} Currently,

only few reports exist that have analyzed the retinal and choroidal vasculature of retinal capillary hemangioblastomas (RCHs) via OCTA,^{4–8} primarily addressing treatment follow-up^{4–7} and more rare classification of the growth type.⁸ Most of these studies were conducted in patients with von Hippel-Lindau disease (VHLD).^{4,6–8}

VHLD is an autosomal dominantly inherited familial phacomatosis that predisposes for different tumors and cysts in multiple organs. Hemangioblastomas in the central nervous system and RCHs are the most common tumors in patients with VHLD^{9–11} and are often the onset of VHLD.¹² The frequency of RCHs in patients with VHLD varies from 49% to 85%.^{13,14} The incidence increases with age, reaching up to 90% in patients older than 60 years.^{15,16} Despite its benign nature and slow growth rates, RCHs can cause complications and visual impairment. Early detection of the RCHs can therefore have a decisive influence on visual prognosis.¹⁷ Conventional ophthalmic screening examinations include ophthalmoscopy, fundus photography, fluorescein angiography (FAG), indocyanine green angiography, optical coherence tomography, and ultrasonography.¹⁸ OCTA, on the other hand, is not yet an integral part of routine controls.

OCTA technology employs motion contrast to image blood flow and works without the need for an intravascular dye application.^{2,3} OCTA technology has developed rapidly, and there are currently two main technologies available: in the previous device generation, light is emitted at a centered wavelength of 840 nm and a spectral analysis (spectral-domain OCT [SD-OCT]) is performed on the interference fringe pattern of the tissue. The most recent development includes swept-source OCT (SS-OCT) technology, which uses a higher scan speed of 100,000 A-scans/s (compared to 68,000 A-scans/s in SD-OCT) and a longer wavelength centered on 1050 nm (compared to 840 nm). Thus, SS-OCT allows deeper penetration into the tissue of 3 mm (compared to 2 mm), with the compromise of a slightly lower axial resolution of 6.3 μm (compared to 5 μm ; personal communication with Zeiss, January 2020) and provides a faster acquisition time.¹⁹

Although both OCTA technologies are possibly applicable to VHLD, an underlying understanding of their characteristics and differences in VHLD imaging is still lacking. Therefore, our study aimed to find new evidence by comparing these methods with regard to RCHs in patients with VHLD.

Methods

Study Design and Population

This is a prospective single-center cross-sectional study. In total, 216 patients with clinically expected VHLD due to VHLD in the family history or the presence of VHLD typical tumors were routinely examined in our eye center between January 2019 and January 2020. From all patients with clinically and/or

genetically confirmed VHLD, signed informed consent was obtained. The study was approved by the institutional Ethics Committee (ID number 360/19) and adhered to the tenets of the Declaration of Helsinki.

Data Collection

Patients underwent a comprehensive ophthalmologic examination including measurement of best-corrected visual acuity and slit-lamp microscopy with fundus examination. If a perfused RCH was clinically detected, fundus photography with an ultra-widefield camera (Optos, Dunfermline, Scotland) was performed and the localization of the RCH was recorded. The tumor size was assessed clinically in relation to the optic disc size as follows: <0.25 disc diameter (DD), 0.25 to 1 DD, 1 to 2 DD, and >2 DD. Assuming an average optic disc diameter of 1.5 mm,²⁰ the clinically assessed tumor size was converted by using the mathematical formula $A = \pi (\text{diameter}/2)^2$ to allow for categorization into the following four groups: (A) <0.11 mm², (B) 0.11 to 1.77 mm², (C) 1.77 to 7.07 mm², and (D) >7.07 mm².

OCTA Imaging

OCTA images were recorded with commercially available OCTA systems: Cirrus 5000 AngioPlex and PLEX Elite 9000 (Carl Zeiss, Meditec, Dublin, CA). The Zeiss Cirrus 5000 AngioPlex uses full-spectrum SD-OCT with a light source wavelength of 840 nm, an A-scan rate of 68,000 A-scans per second, and an A-scan depth of 2.0 mm in tissue (1024 pixels). The Zeiss PLEX Elite 9000 uses full-spectrum SS-OCT with a light source wavelength of 1050 nm, an A-scan rate of 100,000 A-scans per second, and an A-scan depth of 3.0 mm in tissue (1536 pixels). Both OCTA systems use the Optical Microangiography algorithm to decorrelate signal detection. A real-time image stabilizer (FastTrac, a software in the Cirrus 5000 AngioPlex and PLEX Elite 9000 from Carl Zeiss, Meditec, Dublin, CA) ensures for a minimum of movement artifacts. Each patient underwent a 6×6 mm² and, if the RCH was not too large, a 3×3 mm² scan of the complete retinal slab of both devices.

Lesion Inclusion Criteria

We included images of RCHs that were either entirely contained within the 3×3 -mm² and/or 6×6 -mm² OCTA scans. In addition, only images of adequate signal strength of at least 6 (out of 10) indicated by the manufacturer's software without detectable motion artifacts in the area of the RCHs were included.

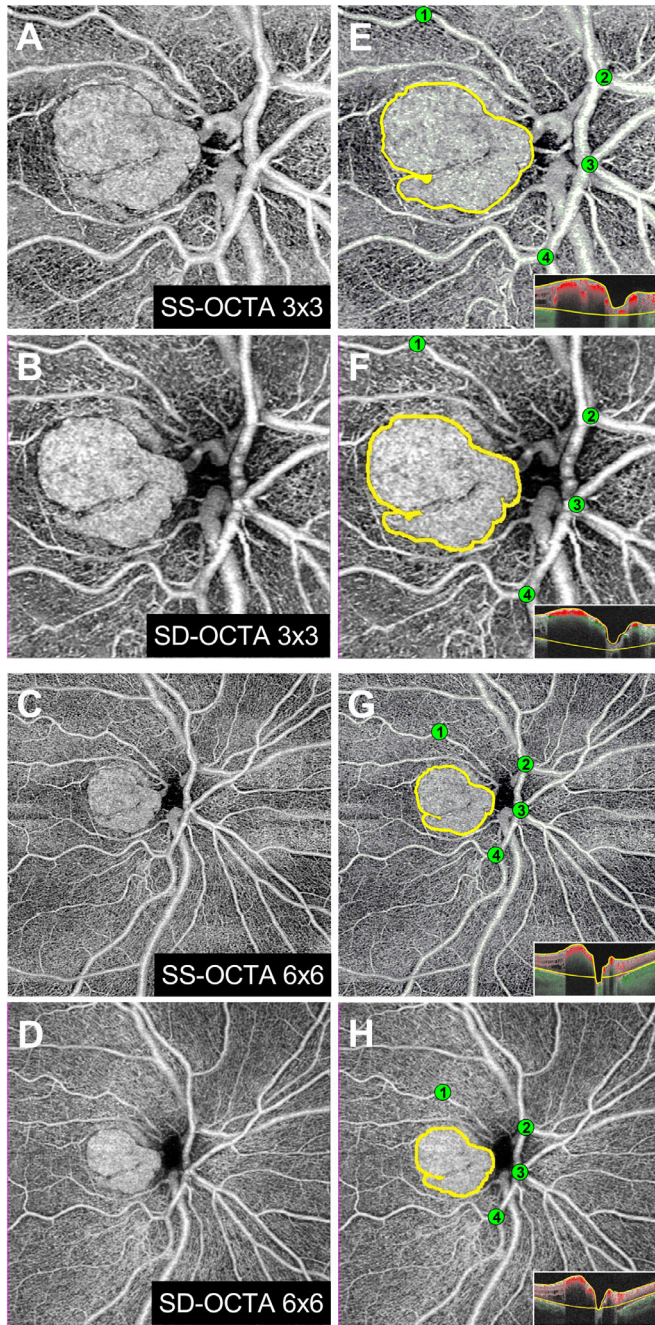


Figure 1. Tumor annotation and area measurement. Tumor areas in corresponding images of the same retinal capillary hemangioblastoma (A–D) were manually outlined (E–H, yellow line). Marker positions (green dots) at corresponding prominent vessel intersections were annotated in all images. On the basis of these marker positions, the images to be compared were aligned.

Image Processing

Two independent graders (MR, AG) outlined the area of the RCH in a self-designed analysis tool programmed in Java and JavaScript as illustrated in Figure 1. Training and familiarization with the annotation tool were performed using OCTA images

from both instruments that were not included in the final grading. It was masked which image technology was displayed. After grading the images separately, the graders reached a consensus outline for each image, and if any lingering disagreements persisted, a third and independent senior grader (SJL) adjudicated the case. When comparing OCTA images that were taken at different times (e.g., images of different sizes taken at the same device or images taken on two different devices), it is not possible to assume exactly the same head position during the images. Consequently, these images cannot simply be overlaid, but a mapping of these images is required to compensate for possible geometric shifts between the images. Therefore, marker positions at corresponding prominent vessel intersections were set in all images, as illustrated in Figure 1. On the basis of these marker positions, the corresponding images were overlaid. After overlaying the corresponding images, the pixel counts within the outlined area were measured and were converted into area measurements in mm^2 .

Verification of Data Repeatability

To verify the repeatability of the data, an additional grader (SN) outlined the area of the RCH as described above. The measured tumor sizes were compared with the consensus outlined tumor area of each image of the graders MR, AG, and JSL.

Statistical Analysis

GraphPad PRISM (GraphPad Software, La Jolla, CA) was used for statistical analysis. A probability (P) value of $\alpha < 0.05$ was considered statistically significant. For the descriptive data analysis, mean \pm standard deviation (SD), median, and minimal and maximal values (range) were calculated. Scatterplots and Bland-Altman plots including analyses of Pearson correlation coefficient (Pearson r) and intraclass correlation coefficient (ICC) were used to determine the reproducibility and variability of the measured areas. Fit spline analyses using four knots for the smoothing spline were conducted to generate the compensation curve. The P value was corrected using Bonferroni correction due to multiple testing. To compare between two groups in a nonparametric way, the Mann-Whitney U test was used. To analyze the influence of signal strength on the measurement of the tumor size, a Cox regression analysis was used, where the image and signal strength were used as constant variables and tumor size as the dependent variable.

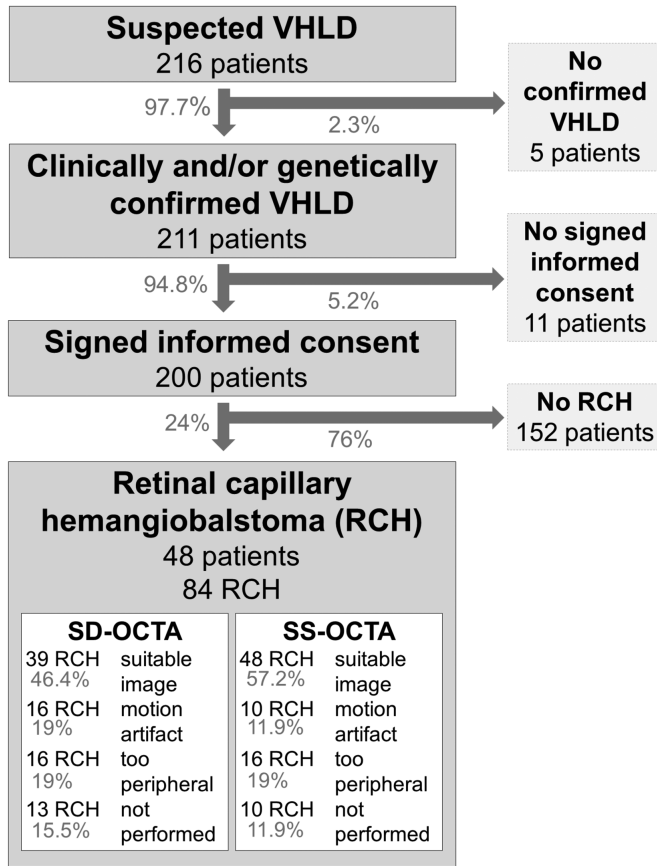


Figure 2. Flowchart of patients and RCHs included in the study.

Results

Patient Characteristics and Detected Retinal Capillary Hemangioblastomas

In total, 216 patients with clinically expected VHL were routinely examined. Five patients were excluded due to neither clinically nor genetically confirmed VHL. Eleven patients were excluded due to missing informed consent. In total, 200 patients were included in the study (male/female, 79/121 patients, 39.5/60.5%). Detailed information about the data collective is illustrated in Figure 2. The mean age at the time of the study examination was 39.4 ± 16.7 years (range, 7–82).

In 48 patients, 84 RCHs were detected, resulting in a mean of 0.42 ± 0.89 tumors/patient ($n = 200$ patients). Thirty-nine of these patients (81.3%) had at least one RCH in one eye and nine patients in both eyes (18.7%). Twenty-five patients (51.1%) had one RCH, 14 patients (29.1%) two RCHs, 6 patients (12.5%) had three RCHs, 2 patients (4.2%) had four RCHs, and 1 patient (2.1%) had five RCHs. Forty-nine of the 84 RCHs (58.3%) were located in the right eye and 35 (41.7%) in the left eye. Twenty-two RCHs (26.2%) in 16 patients were

located peripapillary (11 in the right eye, 11 in the left eye). Eleven patients had one peripapillary RCH in one eye, four patients had two peripapillary RCHs (one patient had one peripapillary RCH in both eyes, and three patients had two peripapillary RCHs in one eye), and one patient had two peripapillary RCHs in one eye and one peripapillary RCH in the other eye. Of the 62 peripheral RCHs, 41 (66.1%) were located in or adjacent to a pretreated area and therefore considered recurrent RCHs, and 21 (33.9%) were primary RCHs.

OCTA Imaging

The localization and clinically assessed tumor sizes of the detected 62 peripheral RCHs are illustrated in Figure 3. Since they overlap, peripapillary RCHs are not shown in Figure 3. Of the 22 peripapillary RCHs, suitable OCTA images of 17 were available. In total, SD-OCTA images of 39 RCHs and SS-OCTA images of 48 RCHs could be used for further analysis. Regarding reasons for exclusion, see Figure 2. All RCHs imaged via SD-OCTA could also be imaged via SS-OCTA. While in both devices, imaging of 16 RCHs was not possible due to peripheral localization, imaging of 10 RCHs in SS-OCTA was not possible due to motion artifacts, which increases with more peripheral localization of the RCHs, compared to imaging of 16 RCHs in SD-OCTA (odds ratio [OR], 0.51; 95% confidence interval, 0.21–1.24, $P = 0.14$, taking only performed imaging of RCHs into account that were not located too peripherally).

Comparison of Clinically Estimated Tumor Size and Tumor Size Measured with OCTA

Clinically, for 22 RCHs, a size <0.25 DD (<0.11 mm²) was estimated; for 15 RCHs, a size between 0.25 and 1 DD (0.11–1.77 mm²); for 8 RCHs, a size between 1 and 2 DD (1.77–7.07 mm²); and for 3 RCHs, a size >2 DD (>7.07 mm²). Of the 48 imaged tumors, mean measured tumor size in OCTA images was 1.60 ± 2.58 mm² (range, 0.01–10.43). Clinically estimated tumor size and tumor size measured in OCTA images showed strong correlation ($r = 0.86$, $P < 0.0001$). In 39 RCHs (81.3%), the clinically estimated tumor size and the tumor size measured in OCTA images were consistent. Seven RCHs (14.5%, six <0.25 DD, one 0.25–1 DD) were clinically estimated larger than measured in OCTA images with a mean difference of 0.34 ± 0.44 mm² (range, 0.01–1.30) and two smaller (4.2%, both 0.25–1 DD), both with a difference of 0.10 mm².

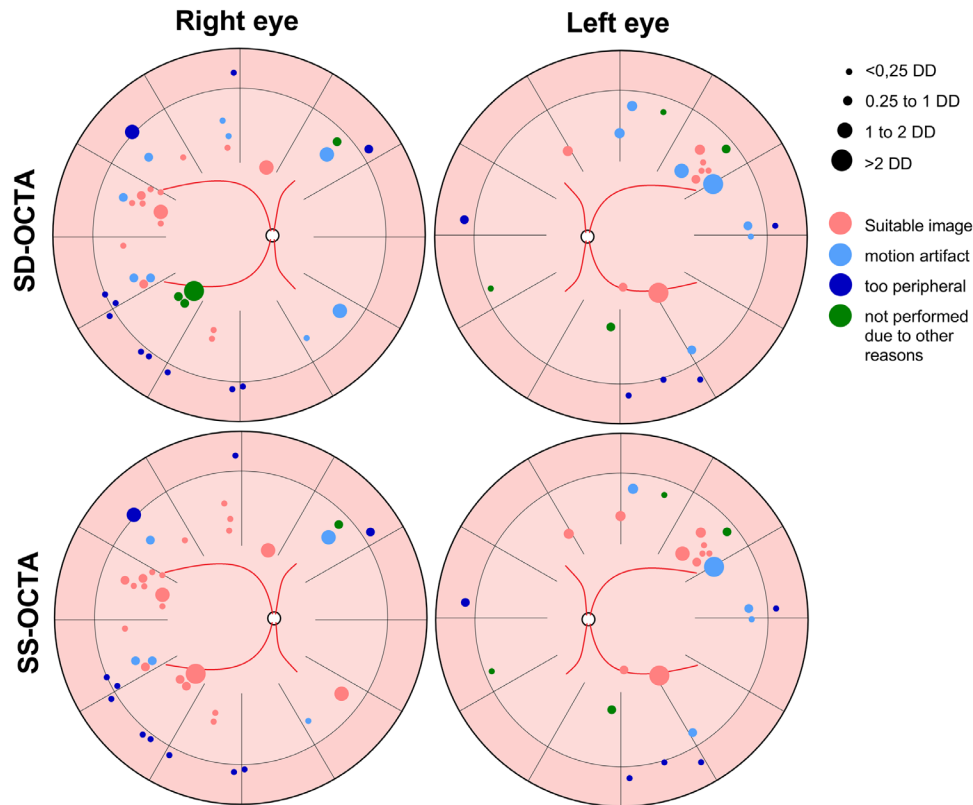


Figure 3. Localization and clinically estimated size of the detected 62 peripheral RCHs. The sizes were determined on the basis of vertical optic disc diameter (DD). In total, 84 RCHs were detected. Twenty-two of these were located peripapillary and are not shown. Suitable OCTA image was available for 17 peripapillary RCHs. For five peripapillary RCHs, OCTA imaging was not performed.

Comparison of Tumor Size Measurements with Different OCTA Devices and Scan Sizes

Scatterplots of the tumor sizes measured in SD-OCTA versus SS-OCTA images and in $3 \times 3\text{-mm}^2$ versus $6 \times 6\text{-mm}^2$ scans are shown in Figures 4A–D. Bland-Altman analyses are shown in Figures 4E–H. Detailed information about the measured tumor sizes in each image is listed in Supplementary Table S1. Although in all area comparisons, correlation is high (all $P < 0.0001$; Figs. 4A–D), in the comparison between SD-OCTA and SS-OCTA (Figs. 4A, 4B), the compensation curve deviates from the bisector proportionately to the size of the tumor. While the measured area of small RCHs matches between both devices, a larger area is measured by SS-OCTA compared to SD-OCTA as the tumor size increases. When comparing the $3 \times 3\text{-mm}^2$ to the $6 \times 6\text{-mm}^2$ scans within a device, the compensation curve corresponds approximately to the bisector of the angle regardless of the tumor size (Figs. 4C, 4D). Bland-Altman plots (Figs. 4E–H) reveal a strong ICC between all compared measured areas (all $P < 0.0001$). Nevertheless, in analyses between both devices, the mean difference in area measurement

deviates from zero in favor for SS-OCTA for large tumors (Figs. 4E, 4F). However, the mean difference of tumor size measured in the $3 \times 3\text{-mm}^2$ compared to the $6 \times 6\text{-mm}^2$ scans within the same device was almost zero, showing no favor for any device, independent of tumor size (Figs. 4G, 4H).

Verification of Data Repeatability

Detailed information about the additional measured tumor sizes in each image for verification of data repeatability is listed in Supplementary Table S1. Bland-Altman analysis and ICC reveal a strong correlation between all compared measured areas (all $\text{ICC} \geq 0.997$, $P < 0.0001$).

Comparison and Influence of Signal Strength When Measuring Tumor Size

Median signal strength of the images conducted by SD-OCTA $3 \times 3\text{-mm}^2$ and $6 \times 6\text{-mm}^2$ scans was both 9 (range, 6–10) and 9 (range, 7–10) for both $3 \times 3\text{-mm}^2$ and $6 \times 6\text{-mm}^2$ SS-OCTA scans. Comparing 3

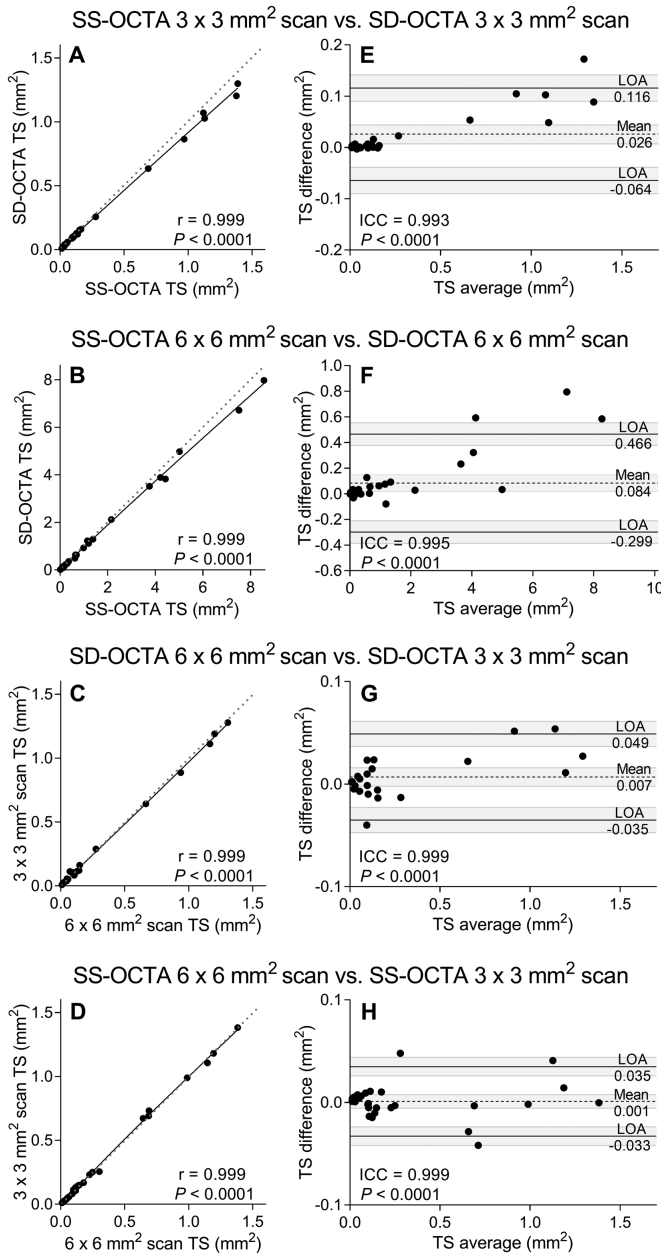


Figure 4. RCH size measured with SS-OCTA versus SD-OCTA. Scatterplots (A–D) and Bland-Altman analyses (E–H) were used. For analyses of SS-OCTA compared to SD-OCTA of 3 × 3-mm² scans, data of 25 RCHs could be used. For analyses of SS-OCTA compared to SD-OCTA of 6 × 6-mm² scans, data of 36 RCHs could be used. For analyses of 3 × 3-mm² compared to 6 × 6-mm² SD-OCTA scans, data of 23 RCHs could be used. For analyses of 3 × 3-mm² compared to 6 × 6-mm² SS-OCTA scans, data of 28 RCHs could be used. (A–D) Fit spline analyses using four knots for the smoothing spline were conducted to generate the compensation curve. Pearson correlation coefficient (r) was analyzed. (E–H) Dashed lines represent average bias between the compared measurements, solid lines represent limits of agreement (LOA), and gray shading represents 95% confidence intervals for the bias and LOAs. ICC was analyzed. TS, tumor size.

× 3–mm² to 6 × 6–mm² scans within the same device and 3 × 3–mm² scans between both devices, no differences in signal strength could be detected ($P > 0.10$). With regards to the comparison of 6 × 6–mm² scans in SS-OCTA with the SD-OCTA, signal strength was higher in SS-OCTA ($P = 0.02$). Using Cox regression analysis where the image and signal strength were used as constant variables and tumor size as the dependent variable, no significant difference in tumor size could be detected (for all analyses of the constant and dependent variables, $P > 0.44$)

Discussion

Retinal capillary hemangioblastomas remain a major cause of visual impairment in patients with VHL. Visual prognosis largely depends on early detection of the RCHs. Therefore, early and accurate OCTA imaging could be a promising, noninvasive, additional tool for a faster RCH diagnosis and monitoring. However, so far, the reports are mainly qualitative, and there is a lack of quantifiable data in VHL. In order to close this gap, we systematically report OCTA image quantification of RCHs in VHL. We were able to show that both current OCTA technologies, SD-OCTA and SS-OCTA, were almost equally suitable to detect and measure the tumor size of RCHs than is possible with current imaging methods.²¹

Tumor size of RCHs, tumor location (juxtapapillary or peripheral), and the location within the retina as well as associated findings (such as extent of subretinal fluid or retinal traction) are all important factors in the choice of treatment for RCHs.¹³ Various treatment modalities have been described for peripheral RCHs. In the literature, careful observation is described for small RCHs (up to 500 microns) not associated with exudation or subretinal fluid and not visually threatening.¹³ In all other peripheral RCHs, laser photocoagulation, cryotherapy, plaque radiotherapy, and vitreoretinal surgery are described as possible treatment options.¹³ In our study, the clinically estimated tumor size strongly correlates with the tumor size measured in OCTA images ($P < 0.0001$). Nevertheless, in 18.7% of tumors, the size differed. Therefore, OCTA can be an additional tool to measure the tumor size. Morphologically endophytic, sessile, and exophytic RCHs can be differentiated.²² Endophytic tumors are located in the inner layers, sessile tumors in the middle layers of the retina, and exophytic tumors in the outer layers. The surgical treatment option is mainly considered for juxtapapillary RCHs with an endophytic growth

pattern due to the accessibility of these lesions,²³ whereas intravitreal bevacizumab (with very limited effectiveness) or verteporfin photodynamic therapy can be considered for sessile and exophytic tumors.²⁴ As shown in a case report by Smid et al.,⁸ OCTA seems to be a valuable tool for juxtapapillary RCH classification. Smid et al.⁸ reported OCTA as a possible tool for follow-up after therapy with intravitreal bevacizumab. OCTA can also be useful for follow-up after laser photocoagulation, as described in a case series by Lang et al.⁷ and in a case report by Chou et al.⁵ Taken together, OCTA can be a helpful diagnostic tool in the diagnosis and follow-up of RCHs. OCTA is able to detect even very small RCHs or recurrent RCHs in pretreated, scarred areas that are sometimes clinically difficult to detect (a representative case is illustrated in Supplementary Fig. S1).

Several studies compared the lesion size of choroidal neovascularization (CNV) imaged with SS-OCTA and SD-OCTA.^{25,26} Both Zhang et al.²⁵ and Miller et al.²⁶ showed larger areas of CNV when imaged by SS-OCTA compared to SD-OCTA. This is consistent with the expected theoretical advantages of the SS-OCTA system since the use of a 1050-nm wavelength (compared to 840 nm in SD-OCTA) reduces optical scattering and absorption from the retinal pigment epithelium (RPE) complex and allows for safe use of higher laser power. Higher laser power results in increased signal from structures below the RPE and therefore a more precise detection of type 1 CNV.²⁵ Comparing the size of RCHs imaged with SS-OCTA and SD-OCTA, we found no difference of the measured tumor size in small tumors. However, with increasing tumor size, our study showed a larger tumor size detected by SS-OCTA too. This might be explained by the fact that RCHs are usually located within the retina, above the RPE.¹³ Therefore, laser penetration into the tissue is equally sufficient in both devices regarding small tumors. Nevertheless, with increasing tumor size, there is an increased shading of deeper lying vessels, as can be seen in the B-scans in Figure 1. Furthermore, a dense blood flow leads to shadowing artifacts of deeper retinal tissue, as this is already known for intraretinal or subretinal fluid.²⁷ Because of its deeper tissue penetration, the SS-OCTA reduces shadowing artifacts²⁸ and detects deeper vessels even in larger tumors, resulting in a better representation of the actual tumor size (for detailed information, see Supplementary Fig. S1). Tumor size and scan dimensions are nominal and vary depending on individual differences in axial length. Since both devices compared in our study use the same assumed model eye axial length, the manufacturer's assumed model eye axial length had no impact on our comparisons.

Although OCTA can be a helpful diagnostic tool in the diagnosis and monitoring of RCHs, there are limitations in imaging RCHs by SD-OCTA and SS-OCTA. Image artifacts in OCTA occur as a result of one or more of the following: the scanning methodology used to generate the motion contrast signal, data processing, movement of the eye, and the intrinsic properties of the eye and pathology³ or increased reflection immediately after laser coagulation of RCHs with a reduced flow signal.⁶ In our study, we excluded 19% of the SD-OCTA images and 11.9% of the SS-OCTA images due to motion artifacts and/or a low signal intensity (Fig. 2). These RCHs were mostly located in the periphery, as illustrated in Figure 3. Although not reaching significance, SS-OCTA images in our study tend to be less influenced by artifacts (OR, 0.51; $P = 0.14$). This is most likely due to the higher A-scan/s speed of the SS-OCTA, which allows a shorter time to capture the image as well as deeper tissue penetration due to the laser properties. To capture a peripheral RCH, the patient has to hold an extreme turn of gaze, which could influence the image acquisition. Furthermore, the period of time needed to capture an image, and thus the amount of time the patient needs to hold the extreme turn of gaze, is shorter with SS-OCTA compared to SD-OCTA. Consequently, peripheral RCHs are easier to capture with SS-OCTA. However, peripheral RCHs can often only be captured by conventionally performed FAG or fundus photography.²⁹ Therefore, OCTA can only be considered a supplementary examination tool.

There are some limitations of our study, such as small sample size in some of our analyses. This is due to the fact that especially SD-OCTA $3 \times 3\text{-mm}^2$ scans were not always possible because of large tumor size or motion artifacts. Although we included only images with a signal strength of at least 6, signal strength significantly varies in the $6 \times 6\text{-mm}^2$ scans of SD-OCTA compared to SS-OCTA. Nevertheless, by using a linear model with the signal strength being the dependent variable when analyzing the difference of the tumor size measurements, we showed that the signal strength had no influence on our analysis. Only one $3 \times 3\text{-mm}^2$ (respectively, $6 \times 6\text{-mm}^2$) scan was taken of each tumor. Unfortunately, our methods and results can therefore not be validated by using a second series of images. Nevertheless, as shown in the Supplementary Table S1, we were able to verify the repeatability of the tumor size measurements using the same series of images.

In summary, with increasing tumor size, a larger area of RCH lesions is measured more sufficiently by SS-OCTA compared to SD-OCTA. Both OCTA imaging technologies were able to display RCHs at a

similar grade and can be useful as additional tools for tumor quantification and monitoring but cannot be used interchangeably.

Acknowledgments

Supported by Verein VHL (von Hippel-Lindau) betroffener Familien e.V. and the Dr. Gabriele Lederle-Stiftung. The sponsor or funding organization had no role in the design or conduct of this research.

Disclosure: **M. Reich**, None; **A. Glatz**, None; **D. Boehringer**, None; **C. Evers**, None; **M. Daniel**, None; **F. Bucher**, None; **F. Ludwig**, None; **S. Nuessle**, None; **W.A. Lagrèze**, None; **P.M. Maloca**, None; **C. Lange**, None; **T. Reinhard**, None; **H. Agostini**, None; **S.J. Lang**, None

References

1. Koustenis A, Jr, Harris A, Gross J, Januleviciene I, Shah A, Siesky B. Optical coherence tomography angiography: an overview of the technology and an assessment of applications for clinical research. *Br J Ophthalmol*. 2017;101:16–20.
2. Ferrara D, Waheed NK, Duker JS. Investigating the choriocapillaris and choroidal vasculature with new optical coherence tomography technologies. *Prog Retin Eye Res*. 2016;52:130–155.
3. Kashani AH, Chen CL, Gahm JK, et al. Optical coherence tomography angiography: a comprehensive review of current methods and clinical applications. *Prog Retin Eye Res*. 2017;60:66–100.
4. Sagar P, Shanmugam PM, Konana VK, Ramanjulu R, Mishra KCD, Simakurthy S. Optical coherence tomography angiography in assessment of response to therapy in retinal capillary hemangioblastoma and diffuse choroidal hemangioma. *Indian J Ophthalmol*. 2019;67:701–703.
5. Chou BW, Nesper PL, Jampol LM, Mirza RG. Solitary retinal hemangioblastoma findings in OCTA pre- and post-laser therapy. *Am J Ophthalmol Case Rep*. 2018;10:59–61.
6. Lang SJ, Evers C, Cakir B, Ludwig F, Lange C, Agostini H. Optical coherence tomography angiography in diagnosis and post-treatment assessment of hemangioblastomas in Hippel-Lindau disease [in German]. *Klin Monbl Augenheilkd*. 2017;234:1146–1153.
7. Lang SJ, Cakir B, Evers C, Ludwig F, Lange CA, Agostini HT. Value of optical coherence tomography angiography imaging in diagnosis and treatment of hemangioblastomas in von Hippel-Lindau Disease. *Ophthalmic Surg Lasers Imaging Retina*. 2016;47:935–946.
8. Smid LM, van Overdam KA, Davidoiu V, et al. Classification and treatment follow-up of a juxtapapillary retinal hemangioblastoma with optical coherence tomography angiography. *Am J Ophthalmol Case Rep*. 2019;15:100472.
9. Conway JE, Chou D, Clatterbuck RE, Brem H, Long DM, Rigamonti D. Hemangioblastomas of the central nervous system in von Hippel-Lindau syndrome and sporadic disease. *Neurosurgery*. 2001;48:55–63.
10. Lonser RR, Glenn GM, Walther M, et al. von Hippel-Lindau disease. *Lancet*. 2003;361:2059–2067.
11. Schmidt D, Agostini HT. Retinal angiomas: an ophthalmological challenge [in German]. *Klin Monbl Augenheilkd*. 2007;224:905–921.
12. Liang X, Shen D, Huang Y, et al. Molecular pathology and CXCR4 expression in surgically excised retinal hemangioblastomas associated with von Hippel-Lindau disease. *Ophthalmology*. 2007;114:147–156.
13. Singh AD, Shields CL, Shields JA. von Hippel-Lindau disease. *Surv Ophthalmol*. 2001;46:117–142.
14. Maher ER, Yates JR, Harries R, et al. Clinical features and natural history of von Hippel-Lindau disease. *Q J Med*. 1990;77:1151–1163.
15. Neumann HP, Wiestler OD. Clustering of features of von Hippel-Lindau syndrome: evidence for a complex genetic locus. *Lancet*. 1991;337:1052–1054.
16. Wittebol-Post D, Hes FJ, Lips CJ. The eye in von Hippel-Lindau disease: *long-term follow-up of screening and treatment: recommendations*. *J Intern Med*. 1998;243:555–561.
17. Chew EY. Ocular manifestations of von Hippel-Lindau disease: clinical and genetic investigations. *Trans Am Ophthalmol Soc*. 2005;103:495–511.
18. Karimi S, Arabi A, Shahraki T, Safi S. Von Hippel-Lindau disease and the eye. *J Ophthalmic Vis Res*. 2020;15:78–94.
19. Wang F, Zhang Q, Deegan AJ, Chang J, Wang RK. Comparing imaging capabilities of spectral domain and swept source optical coherence tomography angiography in healthy subjects and central serous retinopathy. *Eye Vis (Lond)*. 2018;5:19.
20. Crowston JG, Hopley CR, Healey PR, Lee A, Mitchell P, Blue Mountains Eye S. The effect of optic disc diameter on vertical cup to disc

- ratio percentiles in a population based cohort: the Blue Mountains Eye Study. *Br J Ophthalmol*. 2004;88:766–770.
21. Callaway NF, Mruthyunjaya P. Widefield imaging of retinal and choroidal tumors. *Int J Retina Vitreous*. 2019;5(suppl 1):49.
 22. Gass JD, Braunstein R. Sessile and exophytic capillary angiomas of the juxtapapillary retina and optic nerve head. *Arch Ophthalmol*. 1980;98:1790–1797.
 23. Kreusel KM, Bechrakis NE, Neumann HP, Foerster MH. Pars plana vitrectomy for juxtapapillary capillary retinal angioma. *Am J Ophthalmol*. 2006;141:587–589.
 24. Saitta A, Nicolai M, Giovannini A, Mariotti C. Juxtapapillary retinal capillary hemangioma: new therapeutic strategies. *Med Hypothesis Discov Innov Ophthalmol*. 2014;3:71–75.
 25. Zhang Q, Chen CL, Chu Z, et al. Automated quantitation of choroidal neovascularization: a comparison study between spectral-domain and swept-source OCT angiograms. *Invest Ophthalmol Vis Sci*. 2017;58:1506–1513.
 26. Miller AR, Roisman L, Zhang Q, et al. Comparison between spectral-domain and swept-source optical coherence tomography angiographic imaging of choroidal neovascularization. *Invest Ophthalmol Vis Sci*. 2017;58:1499–1505.
 27. Reich M, Bohringer D, Cakir B, et al. Longitudinal analysis of the choriocapillaris using optical coherence tomography angiography reveals subretinal fluid as a substantial confounder in patients with acute central serous chorioretinopathy. *Ophthalmol Ther*. 2019;8:599–610.
 28. Reich M, Boehringer D, Rothaus K, et al. Swept-source optical coherence tomography angiography alleviates shadowing artifacts caused by subretinal fluid [published online April 24, 2020]. *Int Ophthalmol*. doi:10.1007/s10792-020-01376-7
 29. Sagar P, Rajesh R, Shanmugam M, Konana VK, Mishra D. Comparison of optical coherence tomography angiography and fundus fluorescein angiography features of retinal capillary hemangioblastoma. *Indian J Ophthalmol*. 2018;66:872–876.